Tracking episodes of seismicity and gas transport in Campi Flegrei caldera trough seismic, geophysical and geochemical measurements

Flora Giudicepietro 1, Giovanni Chiodini 2, Rosario Avino 1, Giuseppe Brandi 1, Stefano Caliro 1, Walter De Cesare 1, Danilo Galluzzo 1, Antonietta Esposito 1, Adriano La Rocca 1, Domenico Lo Bascio 1, Francesco Obrizzo 1, Salvatore Pinto 1, Tullio Ricci 3, Patrizia Ricciolino 1, Agata Siniscalchi 4, Anna Tramelli 1, Jean Vandemeulebrouck 5, Giovanni Macedonio 1.

1 Istituto Nazionale di Geofisica e Vulcanologia, Osservatorio Vesuviano, Napoli, Italy
2 Istituto Nazionale di Geofisica e Vulcanologia, Bologna, Italy
3 Istituto Nazionale di Geofisica e Vulcanologia, Roma, Italy
4 Dipartimento di Scienze della Terra e Geoambientali, Università degli Studi di Bari ALDO MORO, Bari, Italy,
5 Université Grenoble Alpes, Université Savoie Mont Blanc CNRS, IRD, IFSTTAR, ISTerre, Grenoble, France

Corresponding author:
Flora Giudicepietro, Istituto Nazionale di Geofisica e Vulcanologia, Osservatorio Vesuviano, via Diocleziano 328, 80124, Napoli, Italy
e-mail: flora.giudicepietro@ingv.it

Abstract

This article presents findings from two episodes of seismicity and gas emission that occurred on October 7, 2015 and December 6, 2019 in Campi Flegrei caldera. This caldera has been affected by long-term unrest since 2004. The December 6, 2019 episode, consisting of a swarm of 38 earthquakes (maximum duration magnitude 3.1, the largest between 1984 and March 2020), occurred at the end of a one month period characterized by an increase in the ground uplift rate from 0.19 +/- 0.01 to 0.72 +/- 0.05 mm/day. A sudden increase in the fumarolic tremor amplitude, which is a proxy of gas emission related parameters recorded at Solfatara-Pisciarelli hydrothermal area (e.g. CO2 air concentration), was observed during the seismicity episode. The uplift rate decreased immediately after the swarm (0.10 +/- 0.01 mm/day), whereas the fumarolic tremor amplitude remained higher than that observed prior to the swarm. Through analyzing the time series of uplift recorded in Pozzuoli (central area of the caldera) from differential measurements on tide gauges we were able to identify the 2015 episode. This episode was characterized by increasing uplift rates that culminating in a seismic swarm of 33 earthquakes on October 7, which was followed by decreasing uplift rates. We computed double-difference locations of earthquakes from the two swarms and found that they located along a conduit-like path, coinciding with a high resistivity contrast zone, previously identified by audiomagnetotelluric measurements. The focal mechanisms of the major earthquakes of both swarms indicate fault planes radial with respect to the maximum uplift area. These phenomena can be interpreted as episodes of the volcanic/hydrothermal system pressurization that culminate in an injection of fluids along the conduit-like path, which behaves as a valve that allows fluid discharge and the temporary depressurization of the source region.

Introduction

Campi Flegrei is a caldera that originated in the Campanian Volcanic Zone (Pappalardo and Mastrolorenzo, 2012) about 39 ka b.p., following the great eruption of the Campanian Ignimbrite.

About 15 ka b.p a further caldera forming eruption produced the so-called Neapolitan Yellow Tuff. Before the Monte Nuovo eruption took place in 1538 (Di Vito et al 2016; Liedl et a. 2019), that is the youngest eruption affecting this very active volcanic area, many others had occurred (Smith et al., 2011). Campi Flegrei is a high-risk volcanic district due to its intense urbanization, that includes cities such as Naples and Pozzuoli, now constituting one extended urbanized zone along the Tyrrhenian coastline where more than 2 million people live. (Fig.1).

In general, calderas are very hazardous volcanoes. In comparison to other volcanoes, forecasting calderas evolution is even more puzzling, because they often show prolonged periods of unrest, which are difficult to interpret (Newhall and Dzurisin, 1988; Macedonio et al. 2014; Acocella et al.2015; Chiodini et al., 2016; Giudicepietro et al. 2016; Giudicepietro et al. 2017; Sandri et al. 2017). The current state of Campi Flegrei is a typical example of this behavior as it has been experiencing a long-lasting unrest since 2004, characterized by seismicity, geochemical variations and ground deformation (Chiodini et al., 2017a). Within the general volcanic unrest, the Solfatara-Pisciarelli hydrothermal area, in particular, is showing an increase in its activity, with an escalation in the last decade (Chiodini et al. 2011; 2012; 2015; 2016; 2017b; Cardellini et al., 2017; Giudicepietro et al. 2019, Tamburello et al. 2019). The alert level of Campi Flegrei has been raised from green (base level) to yellow (attention level) by the civil protection authorities since December 2012, because the changes have been interpreted as possibly due to magmatic intrusion (D'Auria et al. 2015a; Trasatti et al. 2015).

The Campi Flegrei's seismicity is intrinsically linked to the dynamics of the caldera and varies over time becoming more frequent in periods when significant ground deformation occurs (D'Auria et al. 2011). Historical research revealed that local earthquakes have affected the Phlegrean area in the past. An intense period of seismic activity began around 1470, several decades before the Monte Nuovo's eruption (1538) and continued after this eruption, culminating with the 1582 earthquake, one of the major events in this area, which probably caused damage in Naples. After that period no noticeable seismicity was reported until the mid-20th century, with the exception of an isolated

seismic event felt in Pozzuoli in 1832, which caused some local damage (Guidoboni and Ciuccarelli, 2011).

Starting in the mid-20th century, repeated bradyseism crises, consisting of ground uplift and typically accompanied by seismicity. These crises occurred around 1950, in 1969-72, and in 1982-85 (Del Gaudio et al. 2010). The latest of these crises produced ground uplift of about 1.8 m and was accompanied by more than 16,000 earthquakes of moderate magnitude (maximum duration magnitude 4.1). These earthquakes seriously damaged the city of Pozzuoli and led to the evacuation of its oldest part.

After the 1982-85 crisis, Campi Flegrei experienced a period of subsidence and stasis of seismicity for about 20 years, interrupted only by a few exceptions (minor uplift in 1989, 1994, 1997, see Orsi et al. 1999, D'Auria et al. 2012). The first signs of unrest appeared in 2000, when the seismicity resumed with VT and LP swarms (Saccorotti et al. 2001), and later in 2004, when a new uplift phase slowly started. Since that time, the vertical displacement has reached a maximum value of ~ 70 cm.

Both the local stress field associated with the ground deformation and the increasing temperature-pressure conditions of the hydrothermal system are thought to control the current seismicity of Campi Flegrei. These concentrations of seismicity are at shallow depths and close to the Solfatara and Pisciarelli fumarolic fields (D'Auria et al. 2015b, Chiodini et al., 2017a, Giudicepietro et al. 2019).

Our analysis is aimed at interpreting two episodes of seismicity and degassing in Campi Flegrei. These occurred on October 7, 2015 and December 6, 2019 and were accompanied by clear evidence of an increase in the hydrothermal activity at the Pisciarelli fumarolic field and by a decrease in the uplift rate. In accordance with recent studies (Chiodini et al., 2017b; Giudicepietro et al., 2019) the fumarolic tremor recorded at Pisciarelli was used as a proxy of the gas flux of the main fumarole and of the intensity of the hydrothermal activity. In addition, seismic (telemetered and stand-alone

stations), geochemical and tide gauge data from the Osservatorio Vesuviano (INGV) monitoring networks (Fig. 1) were used for our analysis.

Fumarolic tremor amplitude as a proxy of the hydrothermal activity

We define the fumarolic tremor amplitude as the RSAM (Endo and Murray, 1991) of the seismic signal (30-minute-long windows of the 5-15 Hz bandpass-filtered vertical component) at the CPIS station located a few meters from the Pisciarelli main vent, which currently represents the main fumarolic emission of the Campi Flegrei caldera (Chiodini et al. 2017b; Giudicepietro et al. 2019). The strict relationship between the RSAM of the CPIS signal and the estimated T-P conditions of the hydrothermal system as inferred by gas-geoindicators has already been highlighted in previous studies (Chiodini et al., 2017b). Here we focus on the variation of the RSAM signal in comparison to the shallow (< 2 km) seismic activity and the air CO_2 concentration close to Pisciarelli emission. Both the shallow seismicity and the air CO_2 concentrations are mainly controlled by hydrothermal processes. Earthquake hypocenters delineate the paths of the fluids moving from a depth of 1–2 km towards the Pisciarelli-Solfatara manifestations (Giudicepietro et al., 2019) and air CO_2 concentrations are linked to the Pisciarelli gas emission. The gas concentration is measured at 40 cm height by an automatic station that measures soil temperatures and CO_2 fluxes (Chiodini et al. (2017b). The station is close to the Pisciarelli vents whose daily CO_2 discharge rate, in recent times, is on the order of hundreds of tons (e.g. 256 ± 85 t d^{-1} and 218 ± 71 t d^{-1} in October 2014, Aiuppa et al., 2015; 578 ± 246 t d^{-1} in May 2017, Queißer et al., 2017; > 600 t d^{-1} in February 2019, Tamburello et al. 2019). The air CO_2 concentration depends on the fumarolic gas flux as well as on other factors, including the distance from the emission, the ground morphology and the local meteorological conditions (Granieri et al., 2013). In our case, the distance from the emission and the ground morphology did not change during the observation period and the meteorologically-controlled variability is attenuated (or eliminated) by averaging the data over long periods (weekly

126 in Fig. 2a and annually in Fig. 3b thus obtaining a signal is mainly dependent on the discharge rate
127 of the fumaroles.
128 Fig. 2 depicts the strict temporal relation linking the RSAM with both the weekly mean of air CO_2
129 concentrations (Fig. 2a) and the cumulative number of shallow earthquakes (Fig. 2b). Similar, but
130 possibly stronger, indications about the unique origin of the three signals is given by the binary
131 plots of Fig. 3, where the annual mean of RSAM (in a log scale) is plotted against the annual mean
132 of the CO_2 air concentration. As it can be noticed in both figures, the amplitude of the different
133 signals increases with time, in conformity with the fast evolution of the Campi Flegrei unrest.
134 In the analysis that follows, the RSAM have been used as a proxy of the variations occurring within
135 the hydrothermal system. With respect to the other variables, RSAM has the advantage of being
136 continuously recorded and is less affected by meteorological conditions, which strongly affect the
137 singular air CO_2 measurements.
138
139 **Tide gauge data analysis**
140 Currently, Campi Flegrei is characterized by ground uplift in the central area (about 70 cm in the
141 last 15 years), which rapidly decreases towards the edges of the caldera. A red circle in Figure 1
142 marks the area of maximum uplift (Iannaccone et al., 2018) that is located in the marine sector of
143 the Campi Flogrei caldera. To show the temporal evolution of the uplift in the central area of the
144 Campi Flegrei caldera, differential measurements from the MISE and POPT tide gauge stations
145 (Fig. 1), which have a sampling frequency of one sample per minute, were used. MISE is located at
146 the caldera border and is subject to an almost negligible uplift, so the MISE-POPT difference is
147 approximately equal to the uplift of the central caldera area. The difference of moving averages of
148 the two time series (MISE-POPT), is useful to eliminate the effects due to the tides, seiches and
149 rough sea, and provides a picture of the uplift temporal evolution. The present study is based on
150 daily averages, selected to obtain one value per day. The period under analysis starts from January

1, 2015 until March 30, 2020 and includes two short-duration increases in uplift rate that preceded two seismic swarms, characterized by relatively high seismic energy (Fig. 4).

Based on the tide gauge data curve (Fig. 4), we calculated the uplift rate before, during and after the two short-duration episodes of increased uplift associated with the two seismic swarms that occurred on October 7, 2015 (Fig. 4a) and December 6, 2019 (Fig. 4b). For the period prior to episode a), from June 15 to August 14, 2015, we found an uplift rate of 0.15 +/- 0.01 mm/day; during episode a), from August 14 to October 7, 2015, the uplift rate was 0.42 +/- 0.01 mm/day, finally, after the episode a), from November 12 to December 31, 2015, the uplift rate decreased to 0.13 +/- 0.01 mm/day. The same analysis was performed for episode b), obtaining an uplift rate of 0.19 +/- 0.01 mm/day for the period prior to the increase in the uplift rate (from August 23 to November 1, 2019), an uplift rate of 0.72 +/- 0.05 mm/day during the phase of increased rate (from November 10 to December 6, 2019), and an uplift rate of 0.10 +/- 0.01 mm/day after the event b) (from December 26, 2019 to February 12, 2020). In 2016, an even longer increase in uplift rate was observed (Fig. 4). As well as the others, this episode was accompanied by seismicity, as shown in Figures 2 and 4; however it did not culminate in a swarm with appreciable seismic energy. The uplift rates for this episode were calculated too, for which a summary is shown in Table 2. It is possible to notice that the highest uplift rate occurred in the 2019 episode, whereas the smallest increase in the uplift rate took place in the 2016 episode and was not accompanied by any swarm with significant cumulative seismic energy. In fact, no sudden step-like increase in the amplitude of the fumarolic tremorwas reported. Hence, we have decided for the present study to focus our attention on episodes a) and b), whose seismic swarms, on the contrary, were characterized by a major seismic energy and were accompanied by a step-like fumarolic tremor amplitude increase, allowing us to recognize a link between seismicity and gas transport in Campi Flegrei caldera.

Seismic data analysis

The seismic catalog of Campi Flegrei in the last ten years shows a gradual increase in the earthquake occurrence (Fig. 2). Considering the temporal evolution of the cumulative seismic

177 energy from January 1, 2015 to March 30, 2020 (Fig. 4) we found two steps at the end of the two
178 short-duration episodes of uplift recognized in the tide gauge data associated to the October 7, 2015
179 and the December 6, 2019 seismic swarms. These sequences were characterized by earthquakes
180 with relatively high duration magnitude (Table 1) compared to the average magnitude (M average =
181 -0.3) of the entire catalog, starting from 2007 (www.ov.ingv.it). The October 7, 2015 swarm
182 includes 33 earthquakes (13 located events; maximum duration magnitude 2.5) whereas the
183 December 6, 2019 swarm consists of 38 earthquakes (16 located events; maximum duration
184 magnitude 3.1, the largest since 1984 until March 2020).
185 We computed double-difference earthquake locations for the two swarms, using the program
186 HypoDD (Waldhauser and Ellsworth, 2000), and found that in both cases the hypocentres were
187 distributed along a conduit-like path (Fig. 5).
188 The focal mechanism of the major earthquakes was also computed for both swarms using
189 FPFIT program (Reasenberg and Oppenheimer, 1985) and results are shown in Fig. 5.
190 The fault plane parameters of the October 7, 2015 09:10 earthquake (duration magnitude 2.5) and
191 the December 6, 2019 00:17 earthquake (duration magnitude 3.1) are reported in Table 3. The two
192 locations and fault plane orientations are similar. The focal mechanisms of the major earthquakes
193 recorded in the two sequences are almost the same, with 90º difference in rake. Both are consistent
194 with normal faults moving mostly on the vertical direction, with the strike radial with respect to the
195 maximum uplift area. This indicates that the same structure could reactivate when the largest
196 earthquakes of the two swarms generated. Mapping the earthquake locations of the two swarms on
197 a resistivity profile (Siniscalchi et al. 2019) that crosses the hydrothermal areas of Solfatara (Gresse
198 et al. 2017) and Pisciarelli (Fig. 6), the hypocenters were found to fall in a zone with significant
199 resistivity contrast, that marks a discontinuity in the physical characteristics of rocks at depth. This
200 observation is consistent with the existence of a conduit-like path characterized by small
201 seismogenic faults, oriented towards the maximum uplift area (red point in Figures 1 and 5), which
202 developed on the structural edge of the Agnano nested caldera (red dotted line in figure 6b).

The two seismic swarms were compared through a cross-correlation analysis (Fig. 7) of all pairs of earthquake onsets (0.8 s) recorded by the vertical component of the CAAM station, installed at Accademia Aeronautica of Pozzuoli (Fig. 1). The events of the October 7, 2015 swarm (0 to 19 in Figure 7) generally show great similarity, whereas the events of the December 6, 2019 swarm (20 to 34 in Figure 7) appear to be more diverse. We decide to focus on the swarms whose events closely resemble each other (black circles in Figure 7). In particular, our analysis revealed great similarity between the events 5, 7, 15 and 18 of the October 7, 2015 swarm and the M3.1 event (number 23) of December 6, 2019 swarm (Fig. 7).

The temporal variations of the fumarolic tremor amplitude at Pisciarelli (CPIS station) around December 6, 2019, show a clear upward march from about 1.0 x10-5 to about 1.2 x 10-5 m/s (offset $\approx 2.0 \times 10^{-6}$ m/s) at the moment of the swarm, followed by a persistent offset which indicates an increase starting on December 6 and lasting several days after the swarm (Fig. 8b). The persistent offset in correspondence of the swarm indicates an increase in gas emission that begins on December 6 and lasts for several days after the swarm. In conjunction with the persistent offset in the fumarolic tremor amplitude, the uplift rate decreased from 0.72 +/- 0.05 mm/day (in the period November 10 - December 6, 2019) to 0.10 +/- 0.01 mm/day after the swarm, and this value remained approximately unaltered until the end of February 2020. A similar temporal evolution of the uplift rate in relation to the swarm occurrence was also observed on October 7, 2015 (Fig. 8a). During the swarm an offset occurred of about 1.9×10^{-6} m/s (from about 1.49×10^{-5} to about 1.68×10^{-5} m/s) in the amplitude of the fumarolic tremor. The correlation between the fumarolic tremor temporal evolution and the uplift rate for the swarm of October 7, 2015 is less evident than for the December 6, 2019 swarm (Fig. 8).

In 2018, an acoustic sensor from the ISTerre laboratory was installed at about 20 m from the Pisciarelli fumarole. This sensor, whose functionalities are described in Grangeon and Lesage (2019), allows for the measurement of acoustic signals in two frequency bands, one in infrasound and the other at higher frequency (MEMS), with a flat frequency response up to 500 Hz. This last

band is used to monitor the acoustic signal emitted by the fumarole, which has a peak at 150Hz. The acoustic energy is averaged over 1 second by an integrator chip, then the rms maximum and average values per minute are recorded on a datalogger.

During the seismic swarm of Dec. 6, 2019, the infrasound band of this sensor did detect earthquakes of magnitude greater than 1, but did not show any noticeable long-term variations, and neither did the MEMS sensor, although the signal variability following the December 6 earthquake series was higher than usual. The averaged standard deviation stepped from 1.5 to about 3.5 (a. u.) after the swarm, so the signal variability increased by a factor of about 2.5, indicating the gas flow to be much more variable than normal.

At the end of December 6, the amplitude of the acoustic signal showed a strong periodic component, with a period of about 40 minutes (Fig.9). Such a periodic transient suggests that the degassing regime becomes pulsatile. This fluid flow instability had been likely produced by the seismic swarm.

Conclusions

The temporal evolution of the fumarolic tremor amplitude compared to the ground uplift before and after the two swarms that occurred on October 7, 2015 and December 6, 2019 (Fig. 8) allowed us to highlight a relationship between changes in the uplift rate, swarm seismicity and hydrothermal activity. The uplift rate increased ahead of both swarms, which were characterized by relatively high magnitude earthquakes, thus revealing a link between the rate of deformation and the release of seismic energy (Fig. 4). The fumarolic tremor, as discussed above (Figs 2 and 3), is a very sensitive indicator of changes in the Solfatara-Pisciarelli hydrothermal system (Chiodini et al. 2017b; Giudicepietro et al. 2019), therefore its sudden increase during the swarms indicates a sudden intensification of the fluid emission in the hydrothermal area of Pisciarelli, which persists after the swarms have ended. In essence, the two seismic sequences under analysis showed a similar progression of events, which can be described as follows: 1) an increase in the uplift rate before the sequence; 2) a swarm with relatively large magnitude earthquakes; 3) an increase in the

255 fumarolic tremor amplitude, and, therefore, in the hydrothermal activity, followed by a decrease in
256 the uplift rate (Figs 4 and 8). This sequence can be interpreted as the effect of the
257 hydrothermal/volcanic system pressurization, which contributes to generate the increase in the
258 uplift rate and the activation of seismogenic structures, located along a conduit-like path (Fig. 5)
259 crossing an area with significant variation of the rock physical properties, as revealed by the
260 resistivity profile carried out by Siniscalchi et al. (2019) (Fig. 6). This is also the region that likely
261 separates a hot gas plume (resistive vertical structure in Fig. 6) from the colder peripheral liquid
262 bearing zone (Siniscalchi et al., 2019). The sudden step in the fumarolic tremor amplitude,
263 particularly evident in the December 6, 2019 swarm, suggests a valve-like mechanism that favors
264 the abrupt increase in the transport of fluids to the surface, through the path where seismicity is
265 concentrated. Tuffs, altered to clays because of the hydrothermal activity, controls this
266 mechanism. The presence of a cap-rock on the top of a vapor-dominated reservoir is well depicted
267 by the shallow low resistivity layer in the Solfatara-Pisciarelli district (Siniscalchi et al., 2019),
268 which overtops a high resistivity plume; furthermore, it is supported by a 3D seismic tomographic
269 reconstruction (Vanorio and Kanitpanyacharoen, 2015). Within this layer, fluid circulation takes
270 place mainly by fracture permeability. In fact, the temporal succession of the earthquakes of the
271 December 6, 2019 swarm shows a propagation of the hypocenters from the bottom to the surface
272 (Fig. 5b).
273 The focal mechanisms of the major earthquakes in the two swarms (locations shown in Figure 5 and
274 6), and the similarity of their waveforms, obtained through cross-correlation (Fig. 7), indicate that
275 similar fault planes were activated in 2015 and 2019. The radiality of the fault planes of the major
276 events with respect to the deformation source position (Iannaccone et al. 2018) and the hypocenter
277 locations of the two studied swarms suggest the existence of seismogenic processes driven by
278 ground deformation and hydrothermal activity. During 2016, a sudden change in fumarolic tremor
279 amplitude associated with a specific seismic swarm was not observed. Moreover, the cumulative
280 energy of the 2016 seismic swarms was small, when compared to the energy of the October 7, 2015

and December 6, 2019 swarms. However, the temporal evolution of the uplift and the number of earthquakes per day in 2016 (Fig. 4) confirm the relationship between the increase in deformation rate and seismicity. This relationship was clearly highlighted by the study of the episodes of seismicity and gas emission that occurred on October 7, 2015 and December 6, 2019, when the fumarolic tremor amplitude increase (Fig. 8) implied an increase in the fluid emission in the Pisciarelli area, thus demonstrating the link between seismicity and hydrothermal activity.

The characteristics of the two swarms here considered, accompanied by a stepwise increase in the amplitude of the fumarolic tremor, put forward the idea that there is a valve-like mechanism capable of inducing an abrupt increase in the hydrothermal activity as well as sudden injections of hot fluids into the conduit-like structure. The described structural characteristics and the current seismicity indicate that this area is critical for monitoring the long-term unrest taking place in the Campi Flegrei caldera.

Data and Resources

This study is base on data provided by the Istituto Nazionale di Geofisica e Vulcanologia (Osservatorio Vesuviano, http://www.ov.ingv.it/ov/it/banche-dati/186-catalogo-sismico-del-vesuvio.html; http://sismolab.ov.ingv.it/sismo/index.php?PAGE=SISMO/last&area=Flegrei).

Supplemental Material has been added as a zip file, containing the following files:

Flegrei-eqk-catalog.dat - The seismic catalog of Campi Flegrei, 2007 – March 31, 2020.

RSAM-Pisciarelli.dat - The RSAM time series of the vertical component of the CPIS station (fumarolic tremor), from January 2010 to March 31, 2020.

hypoDD.reloc - Double-Difference locations of 23 earthquakes.

Flegrei-eqk-catalog.dat - The time series of the differential uplift between the POPT and MISE tide gauges.

Acknowledgements

306 We wish to thank all the many colleagues who have contributed to the monitoring effort on Campi
307 Flegrei. We are particularly indebted to the INGV technical staff ensuring the regular working of
308 the multidisciplinary monitoring networks. We thank Novella Tedesco for revising the English of
309 the manuscript. This work benefited from funds of the EU (DG ECHO) Project EVE n. 826292 and
310 was partially supported by the project INGVFISR-2017 "Sale Operative Integrate e Reti di
311 Monitoraggio del Futuro: l'INGV 2.0". The data used in this study were provided by the Istituto
312 Nazionale di Geofisica e Vulcanologia (Osservatorio Vesuviano). The authors are also grateful to
313 the Italian Presidenza del Consiglio dei Ministri-Dipartimento della Protezione Civile (DPC) for
314 supporting the monitoring activities at Campi Flegrei. This paper does not necessarily represent
315 DPC official opinion and policies.
316

317 **References**

318 Acocella, V., R. Di Lorenzo, C. Newhall, and R. Scandone (2015). An overview of recent (1988-
319 2014) caldera unrest: knowledge and perpectives, *Rev. Geophys.* **53**, no. 3, 896–955,
320 doi:10.1002/2015RG000492.

321 Cardellini, C., G. Chiodini, F. Frondini, R. Avino, E. Bagnato, S. Caliro, M. Lelli, and A. Rosiello
322 (2017). Monitoring diffuse volcanic degassing during volcanic unrests: the case of Campi Flegrei
323 (Italy), *Sci. Rep.* **7**, 6757, doi:10.1038/s41598-017-06941-2.

324 Chiodini, G., R. Avino, S. Caliro, and C. Minopoli (2011). Temperature and pressure gas
325 geoindicators at the Solfatara fumaroles (Campi Flegrei), *Ann. Geophys-Italy* **54**, no. 2, 151–160,
326 doi:10.4401/ag-5002.

327 Chiodini, G., S. Caliro, P. De Martino, R. Avino, and F. Gherardi (2012). Early signals of new
328 volcanic unrest at Campi Flegrei caldera? Insights from geochemical data and physical simulations,
329 *Geology* **40**, 943–946, doi:10.1130/G33251.1.

330 Chiodini, G., J. Vandemeulebrouck, S. Caliro, L. D'Auria, P. De Martino, A. Mangiacapra, and
331 Z. Petrillo (2015). Evidence of thermal-driven processes triggering the 2005-2014 unrest at Campi
332 Flegrei caldera, *Earth Planet. Sci. Lett.* **414**, 58–67, doi:10.1016/j.epsl.2015.01.012.

333 Chiodini, G., A. Paonita, A. Aiuppa, A. Costa, S. Caliro, P. De Martino, V. Acocella, and
334 J. Vandemeulebrouck (2016). Magmas near the critical degassing pressure drive volcanic unrest
335 towards a critical state, *Nat. Commun.* **7**, 13,712, doi:10.1038/ncomms13712.

336 Chiodini, G., J. Selva, E. Del Pezzo, D. Marsan, L. De Siena, L. D'Auria, F. Bianco, S. Caliro,
337 P. De Martino, P. Ricciolino, and Z. Petrillo (2017a). Clues on the origin of post-2000 earthquakes
338 at Campi Flegrei caldera (Italy), *Sci. Rep.* **7**, 4472, doi:10.1038/s41598-017-04845-9.

339 Chiodini, G., F. Giudicepietro, J. Vandemeulebrouck, A. Aiuppa, S. Caliro, W. De Cesare,
340 G. Tamburello, R. Avino, M. Orazi, and L. D'Auria (2017b). Fumarolic tremor and geochemical
341 signals during a volcanic unrest, *Geology* **45**, no. 12, 1131–1134, doi:10.1130/G39447.1.

342 D'Auria, L., F. Giudicepietro, I. Aquino, G. Borriello, C. Del Gaudio, D. Lo Bascio, M. Martini,
343 G. P. Ricciardi, P. Ricciolino, and C. Ricco (2011). Repeated fluid-transfer episodes as a
344 mechanism for the recent dynamics of Campi Flegrei caldera (1989-2010), *J. Geophys. Res.* **116**,
345 B04,313, doi:10.1029/2010JB007837.

346 D'Auria, L., F. Giudicepietro, M. Martini, and R. Lanari (2012). The 4D imaging of the source of
347 ground deformation at Campi Flegrei caldera (southern Italy), *J. Geophys. Res.* B08209,
348 doi:10.1029/2012JB009181.

349 D'Auria, L., S. Pepe, R. Castaldo, F. Giudicepietro, G. Macedonio, P. Ricciolino, P. Tizzani,
350 F. Casu, R. Lanari, M. Manzo, M. Martini, E. Sansosti, and I. Zinno (2015a). Magma injection
351 beneath the urban area of Naples: a new mechanism for the 2012-2013 volcanic unrest at Campi
352 Flegrei caldera, *Sci. Rep.* **5**, no. 13100, 1–11, doi:10.1038/srep13100.

353 D'Auria, L., B. Massa, E. Cristiano, C. Del Gaudio, F. Giudicepietro, G. Ricciardi, and C. Ricco
354 (2015b). Retrieving the stress field within the Campi Flegrei caldera (Southern Italy) through an
355 integrated geodetical and seismological approach, *Pure Appl. Geophys.* **172**, no. 11, 3247–3263,
356 doi:10.1007/s00024-014-1004-7.

357 Del Gaudio, C., I. Aquino, G. P. Ricciardi, C. Ricco, and R. Scandone (2010). Unrest episodes at
358 Campi Flegrei: A reconstruction of vertical ground movements during 1905–2009, *J. Volcanol.*
359 *Geotherm. Res.* **195**, 48–56, doi:10.1016/j.jvolgeores.2010.05.014.

360 Di Vito, M. A., V. Acocella, G. Aiello, D. Barra, M. Battaglia, A. Carandente, C. Del Gaudio,
361 S. de Vita, G. P. Ricciardi, C. Ricco, R. Scandone, and F. Terrasi (2016). Magma transfer at Campi
362 Flegrei caldera (Italy) before the 1538 AD eruption, *Sci. Rep.* **6**, 32,245, doi:10.1038/srep32245.

363 Endo, E. T., and T. Murray (1991). Real-time Seismic Amplitude Measurement (RSAM): a volcano
364 monitoring and prediction tool, *Bull. Volcanol.* **53**, 533–545, doi:10.1007/BF00298154.

365 Giudicepietro, F., G. Macedonio, L. D'Auria, and M. Martini (2016). Insight into vent opening
366 probability in volcanic calderas in the light of a sill intrusion model, *Pure Appl. Geophys.* **173**, no.
367 5, 1703–1720, doi:10.1007/s00024-015-1190-y.

368 Giudicepietro, F., G. Macedonio, and M. Martini (2017). A physical model of sill expansion to
369 explain the dynamics of unrest at calderas with application to Campi Flegrei, *Front. Earth Sci.* **5**,
370 no. 54, 1–11, doi:10.3389/feart.2017.00054.

371 Giudicepietro, F., G. Chiodini, S. Caliro, W. De Cesare, A. M. Esposito, D. Galluzzo, D. Lo Bascio,
372 G. Macedonio, M. Orazi, P. Ricciolino, and J. Vandemeulebrouck (2019). Insight into Campi
373 Flegrei caldera unrest through seismic tremor measurements at Pisciarelli fumarolic field, *Geochem.*
374 *Geophys. Geosyst.* **20**, no. 11, 5544–5555, doi:10.1029/2019GC008610.

375 Grangeon J. and P. Lesage (2019). A robust, low-cost and well-calibrated infrasound sensor for
376 volcano monitoring, J. Volc. Geotherm. Res., 387,
377 https://doi.org/10.1016/j.jvolgeores.2019.106668.

378 Gresse, M., J. Vandemeulebrouck, S. Byrdina, G. Chiodini, A. Revil, T. C. Johnson, T. Ricci,
379 G. Vilardo, A. Mangiacapra, T. Lebourg, J. Grangeon, P. Bascou, and L. Metral (2017). Three-
380 dimensional electrical resistivity tomography of the Solfatara crater (Italy): Implication for the
381 multiphase flow structure of the shallow hydrothermal system, *J. Geophys. Res. Solid Earth* **122**,
382 no. 11, 8749–8768, doi:10.1002/2017JB014389.

383 Guidoboni, E., and C. Ciuccarelli (2011). The Campi Flegrei caldera: historical revision and new
384 data on seismic crises, bradyseisms, the Monte Nuovo eruption and ensuing earthquakes (twelfth
385 century 1582 AD), *Bull. Volcanol.* **73**, 655–677, doi:10.1007/s00445-010-0430-3.

386 Iannaccone, G., S. Guardato, G. P. Donnarumma, P. De Martino, M. Dolce, G. Macedonio,
387 F. Chierici, and L. Beranzoli (2018). Measurement of seafloor deformation in the marine sector of
388 the Campi Flegrei caldera (Italy), *J. Geophys. Res. Solid Earth* **123**, no. 1, 66–83,
389 doi:10.1002/2017JB014852.

390 Liedl, A., G. Buono, G. Lanzafame, S. B. Dabagov, G. Della Ventura, D. Hampai, L. Mancini,
391 A. Marcelli, and L. Pappalardo (2019). A 3D imaging textural characterization of pyroclastic
392 products from the 1538 AD Monte Nuovo eruption (Campi Flegrei, Italy), *Lithos* **340-341**, 316–
393 331, doi:10.1016/j.lithos.2019.05.010.

394 Macedonio, G., F. Giudicepietro, L. D'Auria, and M. Martini (2014). Sill intrusion as a source
395 mechanism of unrest at volcanic calderas, *J. Geophys. Res. Solid Earth* **119**, no. 5, 3986–4000,
396 doi:10.1002/2013JB010868.

397 Newhall, C. G., and D. Dzurisin (1988). *Historical Unrest at Large Calderas of the World*,
398 Department of the Interior, U.S. Geological Survey Bulletin 1855.

399 Orsi, G., L. Civetta, C. Del Gaudio, S. de Vita, M. A. Di Vito, R. Isaia, S. M. Petrazzuoli, G. P.
400 Ricciardi, and C. Ricco (1999). Short-term ground deformations and seismicity in the resurgent
401 Campi Flegrei caldera Italy: an example of active block-resurgence in a densely populated area, *J.*
402 *Volcanol. Geotherm. Res.* **91**, 415–451, doi:10.1016/S0377-0273(99)00050-5.

403 Pappalardo, L., and G. Mastrolorenzo (2012). Rapid differentiation in a sill-like magma reservoir:
404 A case study from the Campi Flegrei caldera, *Sci. Rep.* **2**, 712, doi:10.1038/srep00712.

405 Reasenberg, P. A., and D. Oppenheimer (1985). FPFIT, FPPLOT, and FPPAGE: Fortran computer
406 programs for calculating and displaying earthquake fault-plane solutions, U.S. Geological Survey,
407 Open-File Report **85-739**.

408 Saccorotti, G., F. Bianco, M. Castellano and E. Del Pezzo (2001). The July-August 2000 seismic
409 swarms at Campi Flegrei Volcanic Complex, Italy. Geophysical Research Letters, **28** (13), 2525–
410 2528. https://doi.org/10.1029/2001GL013053

411 Sandri, L., V. Acocella, and C. Newhall (2017). Searching patterns in caldera unrest, *Geochem.*
412 *Geophys. Geosyst.* **18**, 2748–2768, doi:10.1002/2017GC006870.

413 Siniscalchi, A., S. Tripaldi, G. Romano, G. Chiodini, L. Improta, Z. Petrillo, L. D'Auria, S. Caliro,
414 and R. Avino (2019). Reservoir structure and hydraulic properties of the Campi Flegrei geothermal
415 system inferred by audiomagnetotelluric, geochemical, and seismicity study, *J. Geophys. Res. Solid*
416 *Earth* **124**, no. 6, 5336–5356, doi:10.1029/2018JB016514.

417 Smith, V. C., R. Isaia, and N. J. G. Pearce (2011). Tephrostratigraphy and glass compositions of
418 post-15 kyr Campi Flegrei eruptions: implications for eruption history and chronostratigraphic
419 markers, *Quat. Sci. Rev.* **30**, 3638–3660, doi:10.1016/j.quascirev.2011.07.012.

420 Tamburello, G., S. Caliro, G. Chiodini, P. De Martino, R. Avino, C. Minopoli, A. Carandente,
421 D. Rouwet, A. Aiuppa, A. Costa, M. Bitetto, G. Giudice, V. Francofonte, T. Ricci, A. Sciarra,
422 E. Bagnato, and F. Capecchiacci (2019). Escalating CO2 degassing at the Pisciarelli fumarolic

system, and implications for the ongoing Campi Flegrei unrest, *J. Volcanol. Geotherm. Res.* **384**, 151–157, doi:10.1016/j.jvolgeores.2019.07.005.X

Trasatti, E., M. Polcari, M. Bonafede, and S. Stramondo (2015). Geodetic constraints to the source mechanism of the 2011-2013 unrest at Campi Flegrei (Italy) caldera, *Geophys. Res. Lett.* **42**, no. 10, 3847–3854, doi:10.1002/2015GL063621.

Vanorio, T., & Kanitpanyacharoen, W. (2015). Rock physics of fibrous rocks akin to Roman concrete explains uplifts at Campi Flegrei caldera. Science, 349(6248), 617–621, doi:10.1126/science.aab1292.

Waldhauser, F., and W. L. Ellsworth (2000). A double-difference earthquake location algorithm: Method and application to the Northern Hayward Fault, California, *BSSA* **90**, no. 6, 1353–1368.

Full mailing address for each author

Flora Giudicepietro - flora.giudicepietro@ingv.it, Istituto Nazionale di Geofisica e Vulcanologia, Osservatorio Vesuviano, Via Diocleziano 328, 80124, Napoli, Italy

Giovanni Chiodini - giovanni.chiodini@ingv.it, Istituto Nazionale di Geofisica e Vulcanologia, via Franceschini 31, 40128, Bologna, Italy

Rosario Avino - rosario.avino@ingv.it, Istituto Nazionale di Geofisica e Vulcanologia, Osservatorio Vesuviano, Via Diocleziano 328, 80124, Napoli, Italy

Giuseppe Brandi - giuseppe.brandi@ingv.it, Istituto Nazionale di Geofisica e Vulcanologia, Osservatorio Vesuviano, Via Diocleziano 328, 80124, Napoli, Italy

Stefano Caliro - stefano.caliro@ingv.it, Istituto Nazionale di Geofisica e Vulcanologia, Osservatorio Vesuviano, Via Diocleziano 328, 80124, Napoli, Italy

Walter De Cesare - walter.decesare@ingv.it, Istituto Nazionale di Geofisica e Vulcanologia, Osservatorio Vesuviano, Via Diocleziano 328, 80124, Napoli, Italy

Danilo Galluzzo - danilo.galluzzo@ingv.it, Istituto Nazionale di Geofisica e Vulcanologia, Osservatorio Vesuviano, Via Diocleziano 328, 80124, Napoli, Italy

Antonietta Esposito - antonietta.esposito@ingv.it, Istituto Nazionale di Geofisica e Vulcanologia, Osservatorio Vesuviano, Via Diocleziano 328, 80124, Napoli, Italy

Adriano La Rocca - adriano.larocca@ingv.it, Istituto Nazionale di Geofisica e Vulcanologia, Osservatorio Vesuviano, Via Diocleziano 328, 80124, Napoli, Italy

Domenico Lo Bascio - domenico.lobascio@ingv.it, Istituto Nazionale di Geofisica e Vulcanologia, Osservatorio Vesuviano, Via Diocleziano 328, 80124, Napoli, Italy

Francesco Obrizzo - francesco.obrizzo@ingv.it, Istituto Nazionale di Geofisica e Vulcanologia, Osservatorio Vesuviano, Via Diocleziano 328, 80124, Napoli, Italy

Salvatore Pinto - tullio.ricci@ingv.it, Istituto Nazionale di Geofisica e Vulcanologia, Osservatorio Vesuviano, Via Diocleziano 328, 80124, Napoli, Italy

Tullio Ricci - patrizia.ricciolino@ingv.it, Istituto Nazionale di Geofisica e Vulcanologia, via di Vigna Murata 605, 00143, Roma, Italy

Agata Siniscalchi - sinia59@gmail.com, Dipartimento di Scienze della Terra e Geoambientali, Università degli Studi di Bari ALDO MORO, via Orabona 4, 70125, Bari, Italy

Anna Tramelli - anna.tramelli@ingv.it, Istituto Nazionale di Geofisica e Vulcanologia, Osservatorio Vesuviano, Via Diocleziano 328, 80124, Napoli, Italy

Jean Vandemeulebrouck - jean.vandemeulebrouck@univ-smb.fr, Université Grenoble Alpes, Université Savoie Mont Blanc CNRS, IRD, IFSTTAR, ISTerre, F-73376 Le Bourget du Lac, France

Giovanni Macedonio - giovanni.macedonio@ingv.it, Istituto Nazionale di Geofisica e Vulcanologia, Osservatorio Vesuviano, Via Diocleziano 328, 80124, Napoli, Italy

Tables

Table 1 Earthquakes of the two examined swarms with magnitude > 1.5. The first earthquake belongs to the December 6, 2019 swarm, whereas the others five earthquakes belong to the October 7, 2015 swarm. For a complete list of earthquakes, see the file named “hypoDD.reloc” in the electronic supplement to this article.

Origin Time (UTC)	Latitude°	Longitude°	Depth (m)	Magnitude
2019-12-06 00:17:23.78	40.831169	14.148144	2442	3.1
2015-10-07 09:10:50.68	40.823462	14.147877	1600	2.5
2015-10-07 08:13:51.19	40.824683	14.145212	2365	2.3
2015-10-07 07:54:13.49	40.825785	14.145338	2285	2.0
2015-10-07 07:37:40.70	40.825317	14.145431	2252	2.2
2015-10-07 07:31:33.05	40.824910	14.148073	1776	1.9

474

475 Table 2 Uplift rate before, during and after the two uplift rate increase episodes shown in Fig.4 (*a*
476 and *b*) and in 2016.

Episode	**period before** (yy/mm/dd)	**dz/dt before** (mm/day)	**period during** (yy/mm/dd)	**dz/dt during** (mm/day)	**period after** (yy/mm/dd)	**dz/dt after** (mm/day)
Episode a)	15-06-15 15-08-14	0.15 +/- 0.01	15-08-14 15-10-07	0.42 +/- 0.01	15-11-12 15-12-31	0.13 +/- 0.01
Episode 2016	16-01-01 16-04-05	0.19 +/- 0.01	16-04-05 16-08-08	0.32 +/- 0.01	16-08-08 16-12-31	0.17+/- 0.01
Episode b)	19-08-23 19-11-01	0.19 +/- 0.01	19-11-10 19-12-06	0.72 +/- 0.05	19-12-26 20-02-12	0.10 +/- 0.01

477

478 Table 3 Origin time, magnitude and focal mechanism parameters of the two major earthquakes of
479 the two seismic swarms (2015 and 2019).

Date	M	Strike°	Dip°	Rake°
2015-10-07 09:10	2.5	235+/-5	85+/-5	-60+/-10
2019-12-06 00:17	3.1	229+/-10	85+/-10	-120+/-5

480

481 **List of Figure Captions**

482 Figure 1. On the left, the map of Campi Flegrei caldera (red line indicates the caldera rim). The
483 yellow triangles indicate the seismic network stations. The light blue stars indicate the tide gauge

484 used in the article. The orange circle highlights the Solfatara - Pisciarelli hydrothermal area. The
485 red triangle on the edge of the orange circle indicates the CAAM station used for cross-correlation
486 analysis (see below). The red circle marks the maximum uplift area (Iannaccone et al. 2018).). On
487 the right, a detailed map of the Pisciarelli area with the location of CPIS seismic station and
488 FLXOV8 geochemical station can be found.
489
490 Figure 2. RSAM (gray) compared with (a) the weekly means of air CO_2 concentrations at Pisciarelli
491 site (vertical axis in ppmv) and (b) the cumulative number of earthquakes, since 2000, (vertical
492 axis) occurring at depth < 2 km in the hydrothermal area. RSAM is expressed in counts. For the
493 RSAM time series of the vertical component of the CPIS station, see the file named "RSAM-
494 Pisciarelli.dat" in the electronic supplement to this article.
495
496 Figure 3. Binary plots of (a) the air CO2 concentration and (b) the earthquake frequency vs. the log
497 of RSAM. Air CO2 concentration and log RSAM refer to annual mean values.
498
499 Figure 4. Uplift, earthquake occurrence and seismic energy in January, 2015 – March, 2020
500 interval. The red curve indicates the differential uplift between the POPT and MISE tide gauges
501 (blue stars in Fig. 1). The inside tick labels of the left vertical axis indicate the differential uplift in
502 meters. The cyan points and the black line represent the cumulative seismic energy computed
503 through the formula: Log E = 9.9 + 1.9 M (right axis). The histogram represents the earthquake
504 daily frequency (left axis). The red arrows mark the October 7, 2015 swarm (detail in box a) and the
505 December 6, 2019 swarm (detail in box b), which correspond to the main steps in the cumulative
506 energy curve. For the differential measurements between the POPT and MISE tide gauges, see the
507 file named "tide-gauge-popt-mise.dat" in the electronic supplement to this article. For the seismic
508 catalog of Campi Flegrei, see the file named "Flegrei-eqk-catalog.dat" in the electronic supplement
509 to this article.

Figure 5. Focal mechanism of the major earthquake (October 7, 2015 09:10) and Double-Difference locations of the 2015 swarm (a) and focal mechanism of the major earthquake (December 6, 2019 00:17) and Double-Difference locations of the 2019 swarm (b). The red point indicates the maximum uplift area (Iannaccone et al. 2018). Note that both fault planes of the major events of the two swarms are approximately radial with respect to the maximum uplift area.

Figure 6. Resistivity profile (a) and double-difference locations of the earthquakes of the 7 October 2015 (yellow circles) and 6 December 2019 (black circles) swarms. Panel b shows the edge of Agnano's nested caldera (dashed red line) and the trace of the resistivity profile. The epicenters of the earthquakes of the two swarms are shown on the map. Panel c shows the distribution of the hypocenters of the swarms with depth, in a 3D view. The red line indicates the trace of the resistivity profile.

Figure 7 Cross-correlation of the events of 2015 swarm (from 0 to 19) and the 2019 swarm (from 20 to 34). The color scale, from blue to dark red passing through green and yellow, represents the correlation that varies between 0 (blue) and 1 (dark red). The black lines separate the events belonging to the two swarms. The black circles highlight 4 events of the 2015 swarm that have high similarity with the event of 00:17 on 6 December 2019 (M 3.1). On the right, the waveforms of the onset of these events.

Figure 8 Uplift (in blue) and fumarolic tremor amplitude (in red) around the swarms of October 7, 2015 (a) and December 6, 2019 (b). In both plots, the black vertical line marks the swarm occurrence time.

535 Figure 9 : Acoustic signal amplitude, measured 20 m away from the Pisciarelli fumarole between

536 20:00 and 22:30 (UTC) on 6 December 2019.

537

538 **Figures**

539

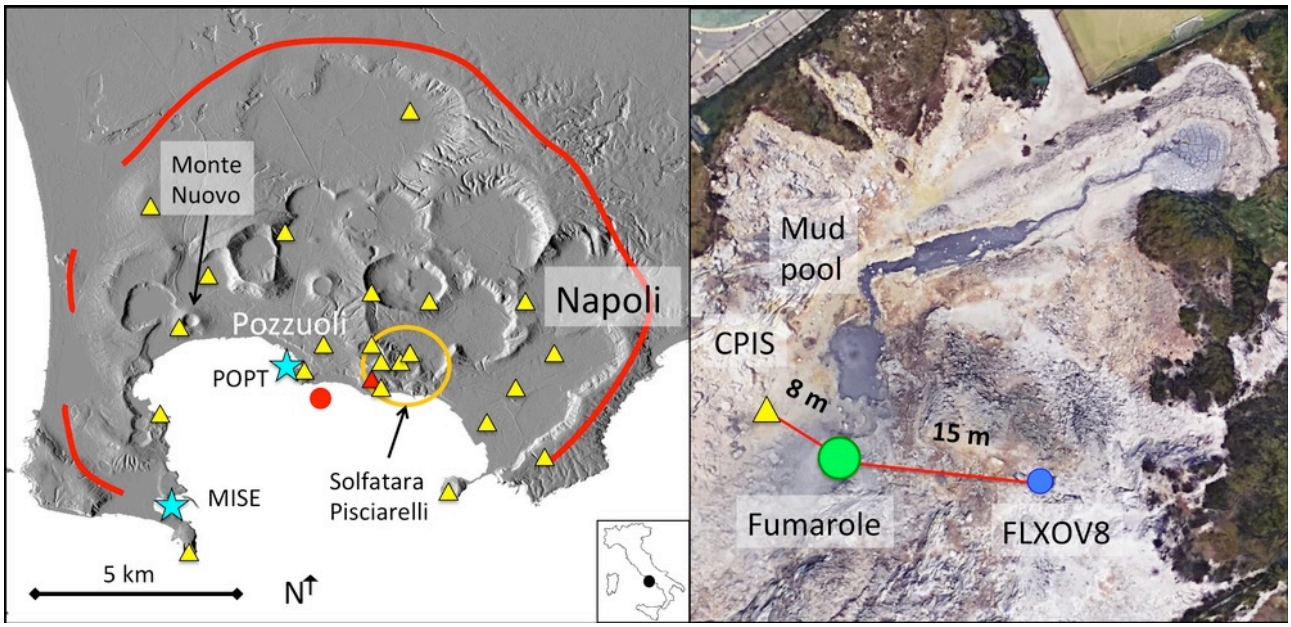

540 Figure 1. On the left, the map of Campi Flegrei caldera (the red line indicates the caldera rim). The

541 yellow triangles indicate the stations of the seismic network. The light blue stars indicate tide gauge

542 used in the article. The orange circle highlights the Solfatara - Pisciarelli hydrothermal area. The red

543 triangle on the edge of the orange circle indicates the CAAM station used for cross-correlation analysis

544 (see below). The red circle marks the maximum uplift area (Iannaccone et al. 2018). On the right, a

545 detailed map of the Pisciarelli area with the location of CPIS seismic station and FLXOV8

546 geochemical station.

547

548

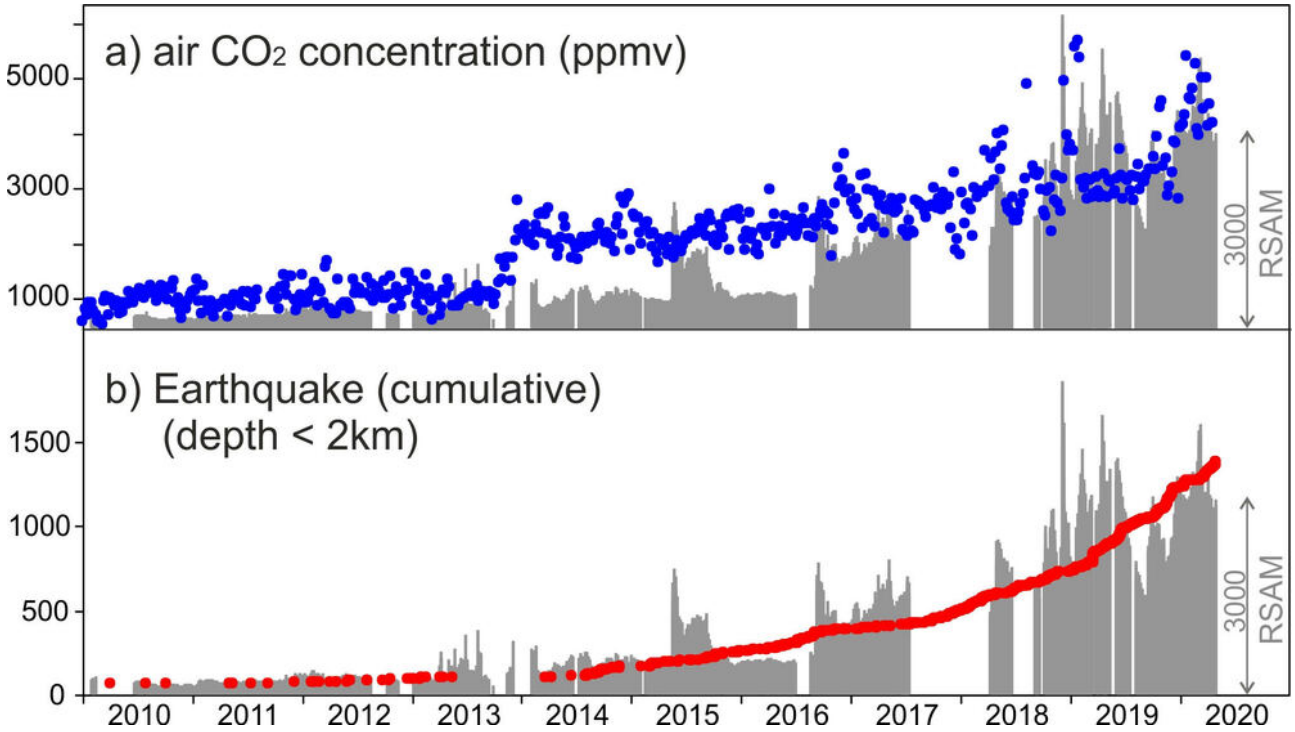

549
550 Figure 2. RSAM (gray) compared with (a) the weekly means of air CO_2 concentrations at Pisciarelli
551 site (vertical axis in ppmv) and (b) the cumulative number of earthquakes, since 2000, (vertical
552 axis) occurring at depth < 2 km in the hydrothermal area. RSAM is expressed in counts. For the
553 RSAM time series of the vertical component of the CPIS station, see the file named "RSAM-
554 Pisciarelli.dat" in the electronic supplement to this article.

555

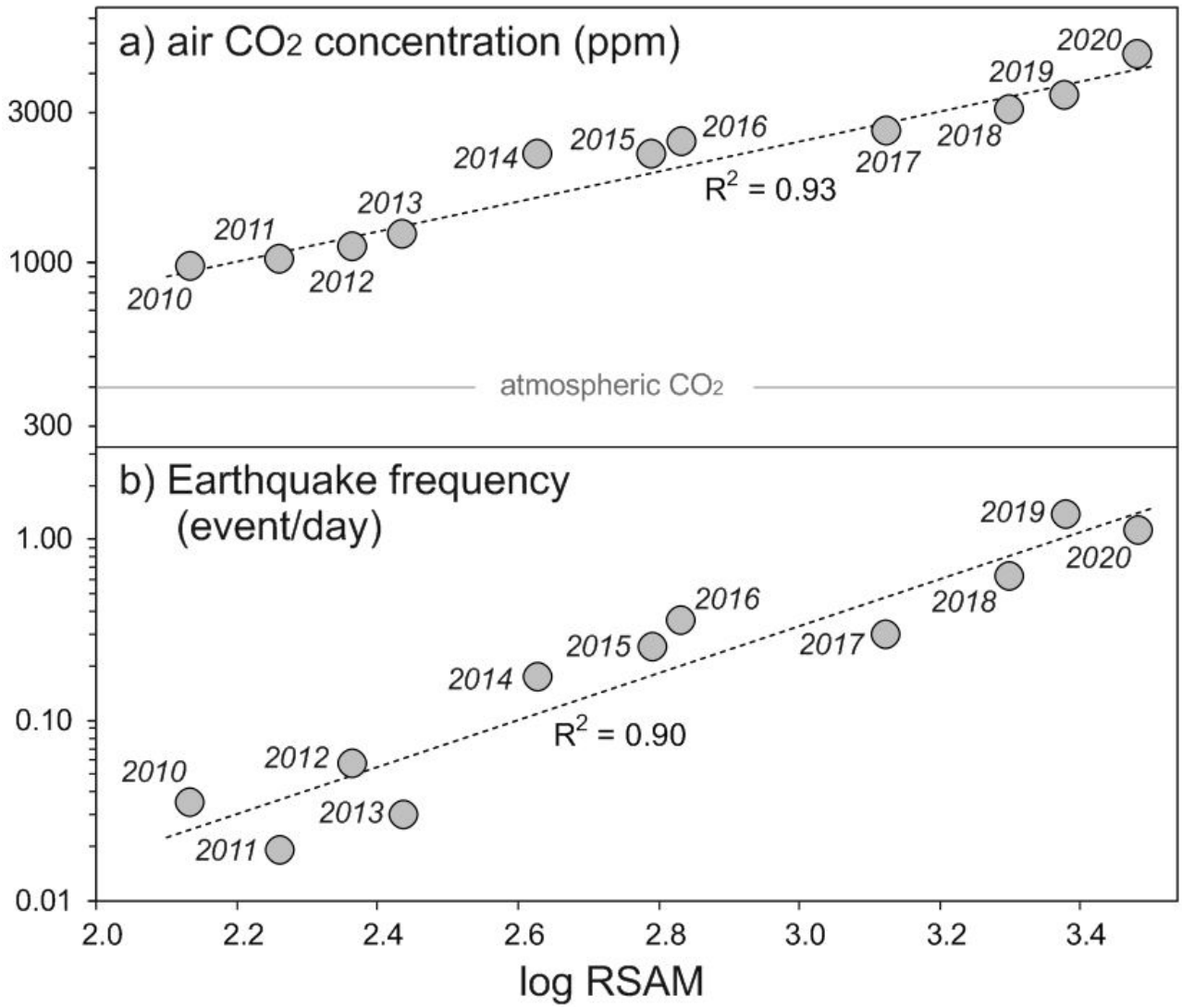

Figure 3. Binary plots of (a) the air CO2 concentration and (b) the earthquake frequency vs. the log of RSAM. Air CO2 concentration and log RSAM refer to annual mean values.

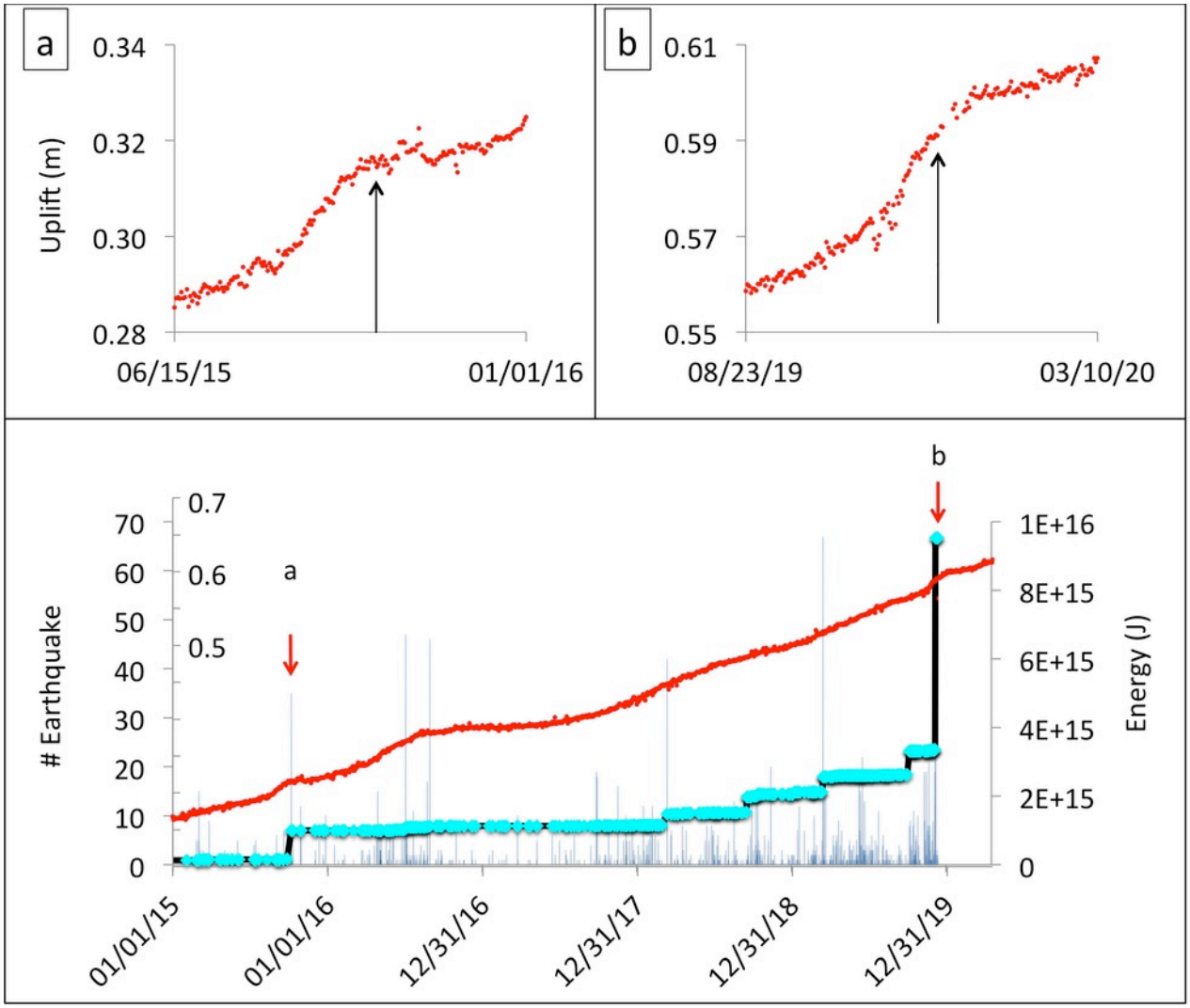

Figure 4. Uplift, earthquake occurrence and seismic energy in January, 2015 – March, 2020 interval. Red curve indicates the differential uplift between the POPT and MISE tide gauges (blue stars in Fig. 1). The inside tick labels of the left vertical axis indicate the differential uplift in meters. The cyan points and the black line represent the cumulative seismic energy computed through the formula: Log E = 9.9 + 1.9 M (right axis). The histogram represents the earthquake daily frequency (left axis). The red arrows mark the October 7, 2015 swarm (detail in box a) and the December 6, 2019 swarm (detail in box b), which correspond to the main steps in the cumulative energy curve. For the differential measurements between the POPT and MISE tide gauges, see the file named "tide-gauge-popt-mise.dat" in the electronic supplement to this article. For the seismic catalog of Campi Flegrei, see the file named "Flegrei-eqk-catalog.dat" in the electronic supplement to this article.

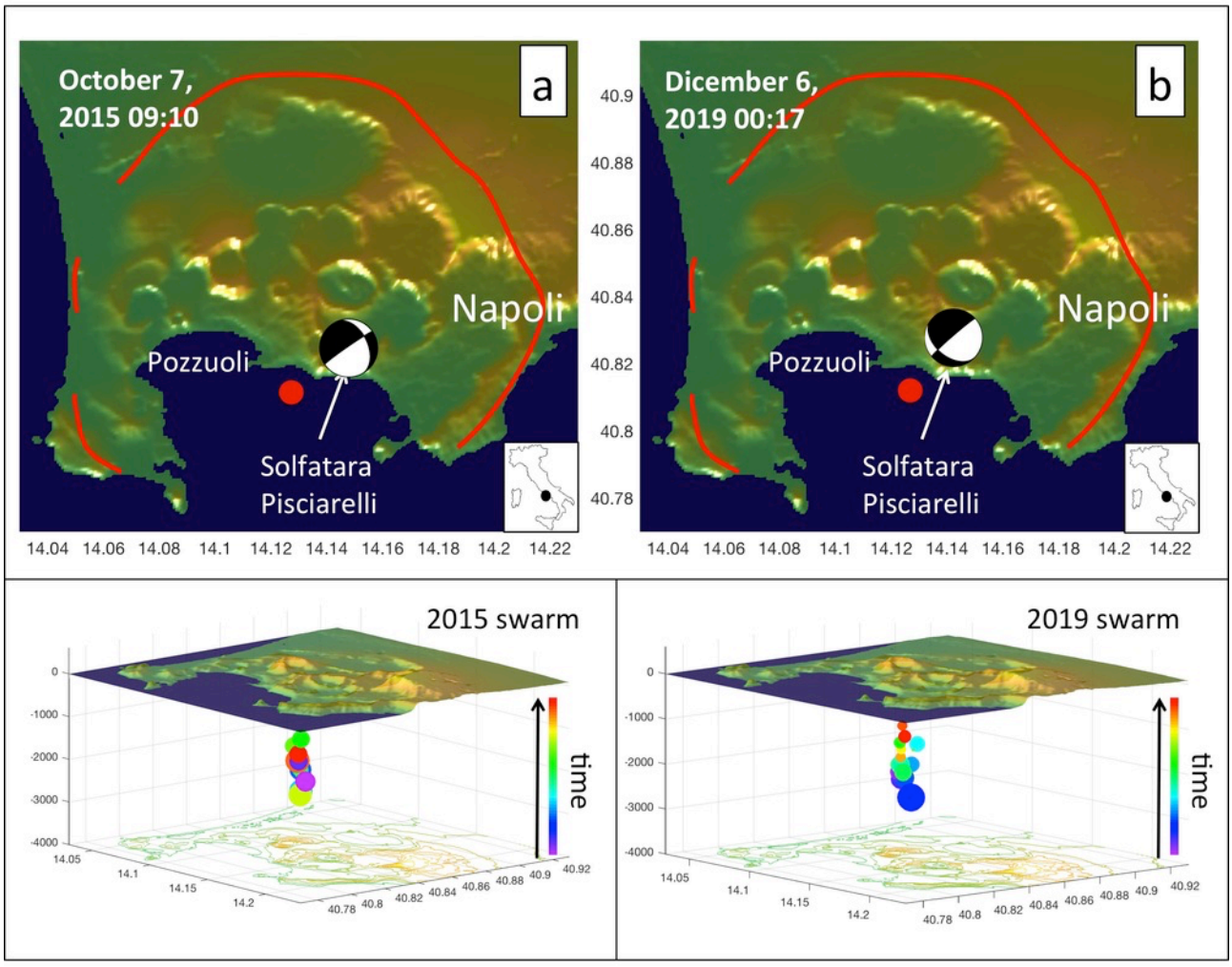

Figure 5. Focal mechanism of the major earthquake (October 7, 2015 09:10) and Double-Difference locations of the 2015 swarm (a) and focal mechanism of the major earthquake (December 6, 2019 00:17) and Double-Difference locations of the 2019 swarm (b). The red point indicates the maximum uplift area (Iannaccone et al. 2018). Note that both fault planes of the major events of the two swarms are approximately radial with respect to the maximum uplift area.

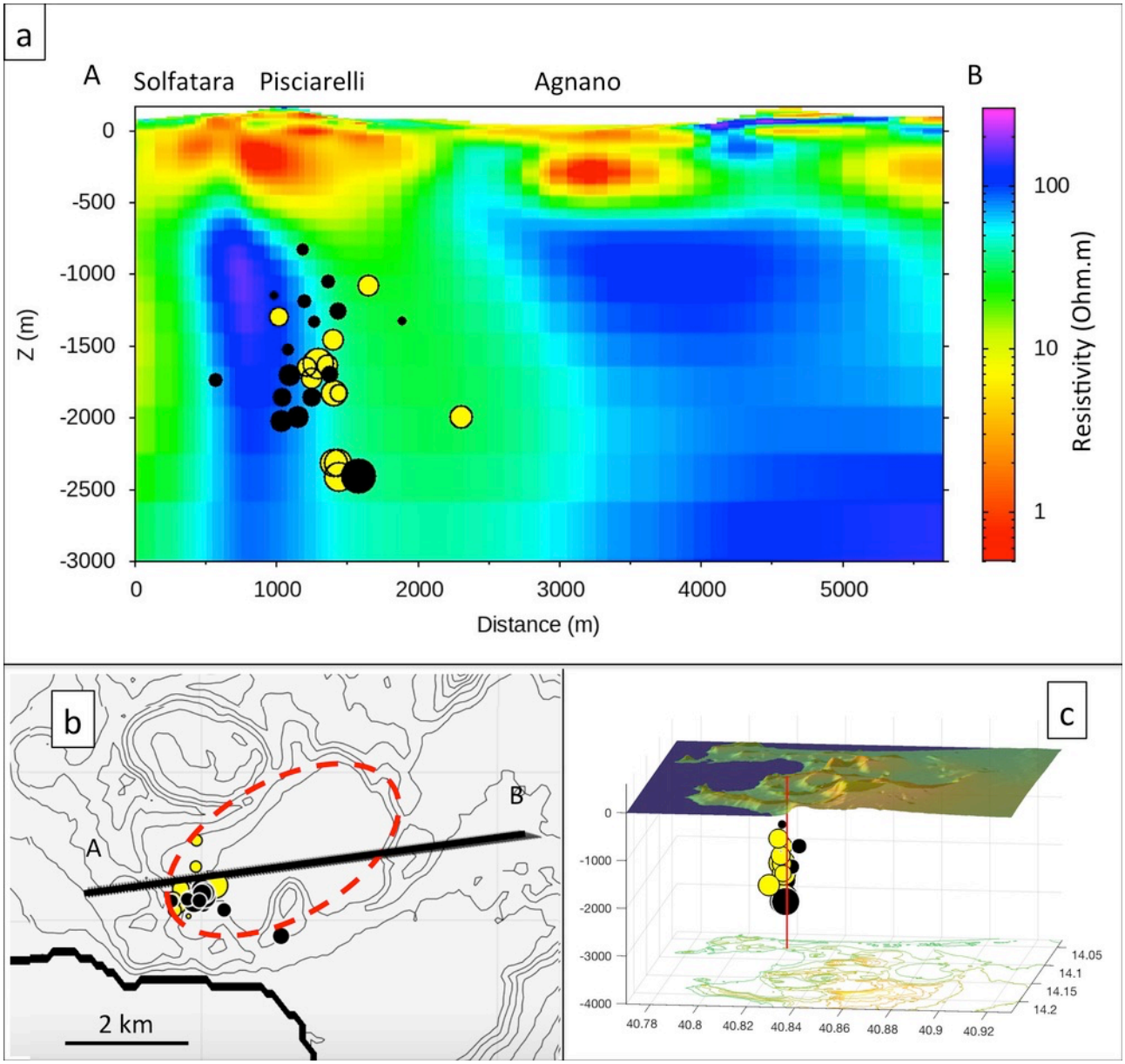

Figure 6. Resistivity profile (a) and double-difference locations of the earthquakes of the 7 October 2015 (yellow circles) and 6 December 2019 (black circles) swarms. Panel b shows the edge of Agnano's nested caldera (dashed red line) and the trace of the resistivity profile. The epicenters of the earthquakes of the two swarms are shown on the map. Panel c shows the distribution of the hypocenters of the swarms with depth, in a 3D view. The red line indicates the trace of the resistivity profile.

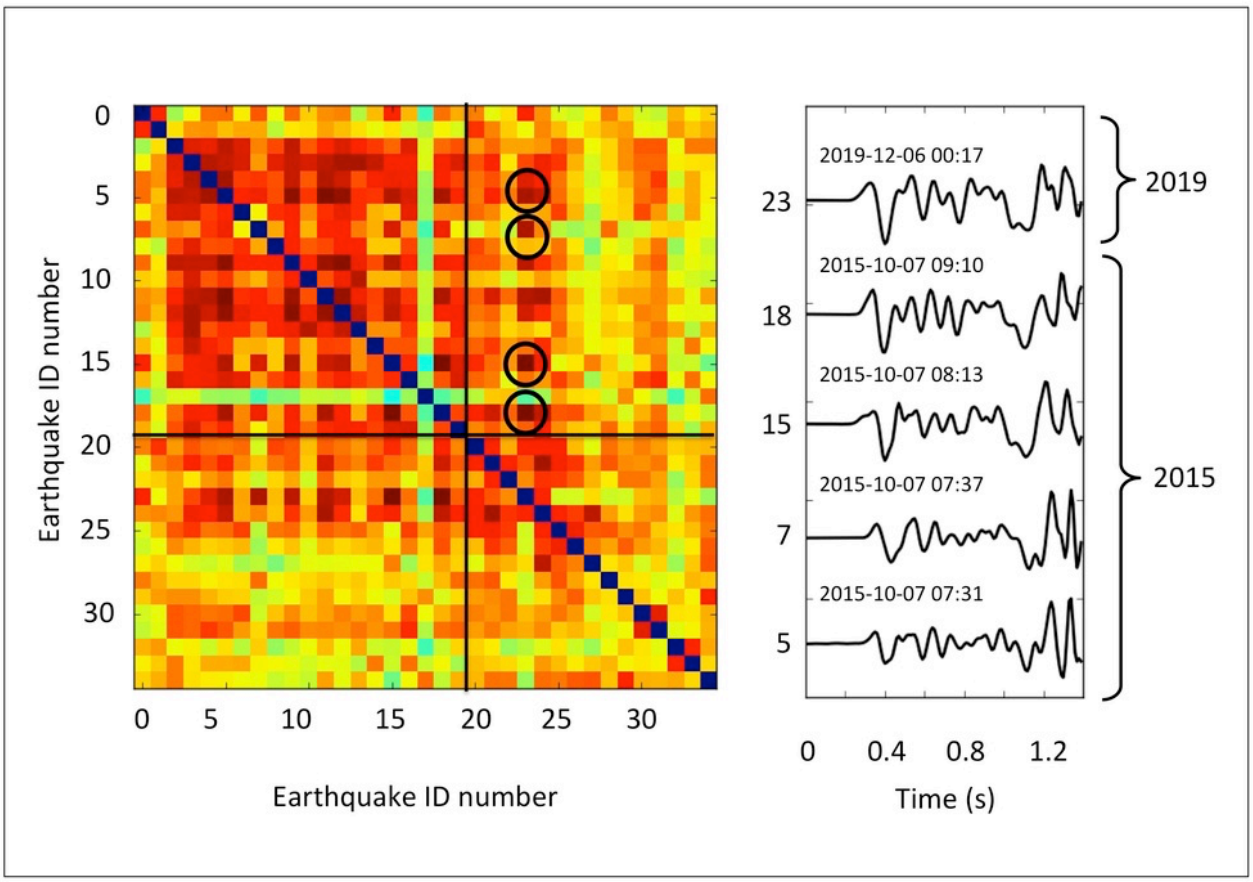

Figure 7 Cross-correlation of the events during the 2015 (from 0 to 19) and the 2019 (from 20 to 34) swarms. The color scale, from blue to dark red passing through green and yellow, represents the correlation that varies between 0 (blue) and 1 (dark red). The black lines separate the events belonging to the two swarms. The black circles highlight 4 events of the 2015 swarm that have high similarity with the event of 00:17 on 6 December 2019 (M 3.1). On the right, the waveforms of the onset of these events.

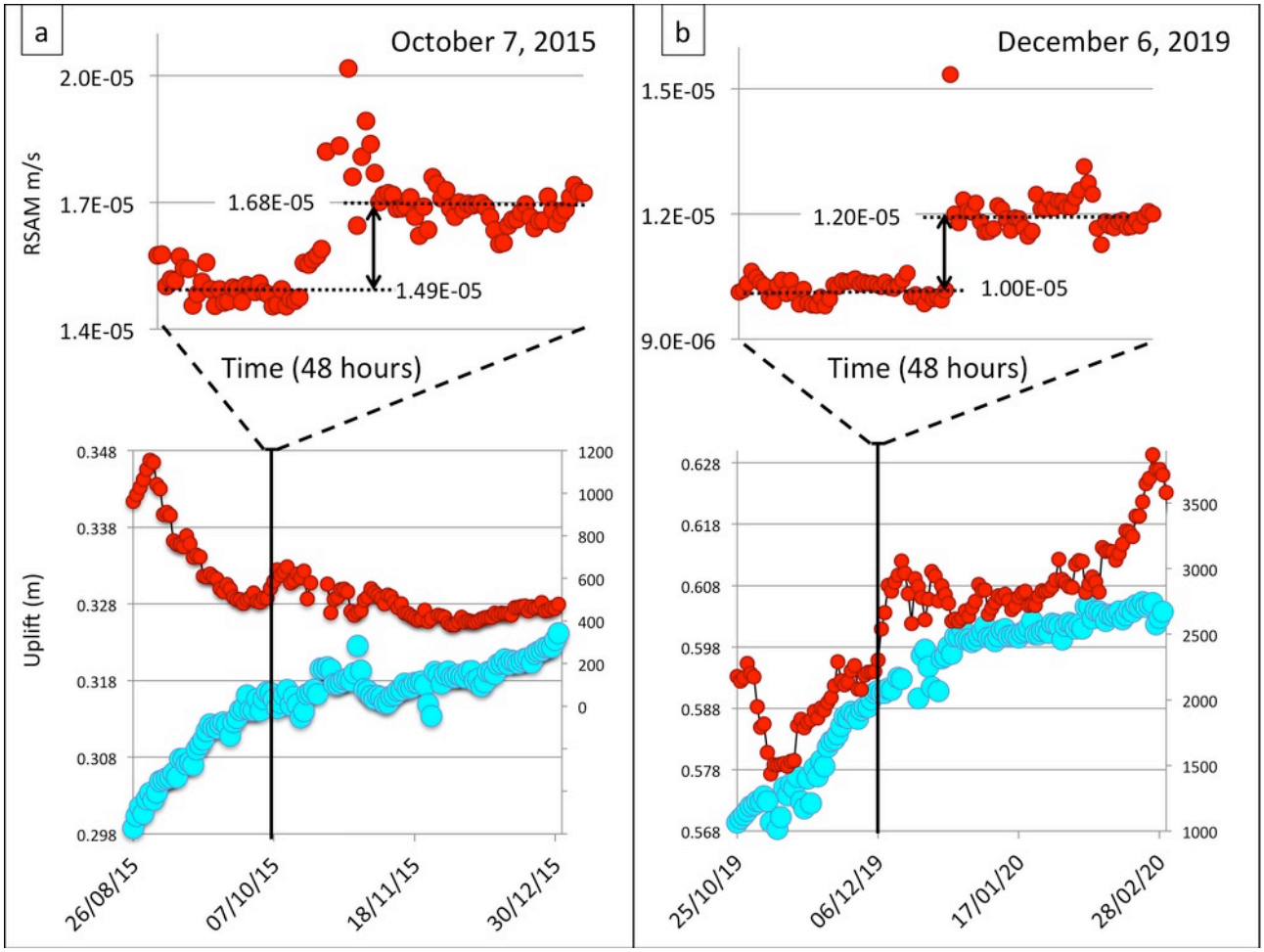

Figure 8 Uplift (in blue) and fumarolic tremor amplitude (in red) around the swarms of October 7, 2015 (a) and December 6, 2019 (b). In both plots, the black vertical line marks the swarm occurrence time.

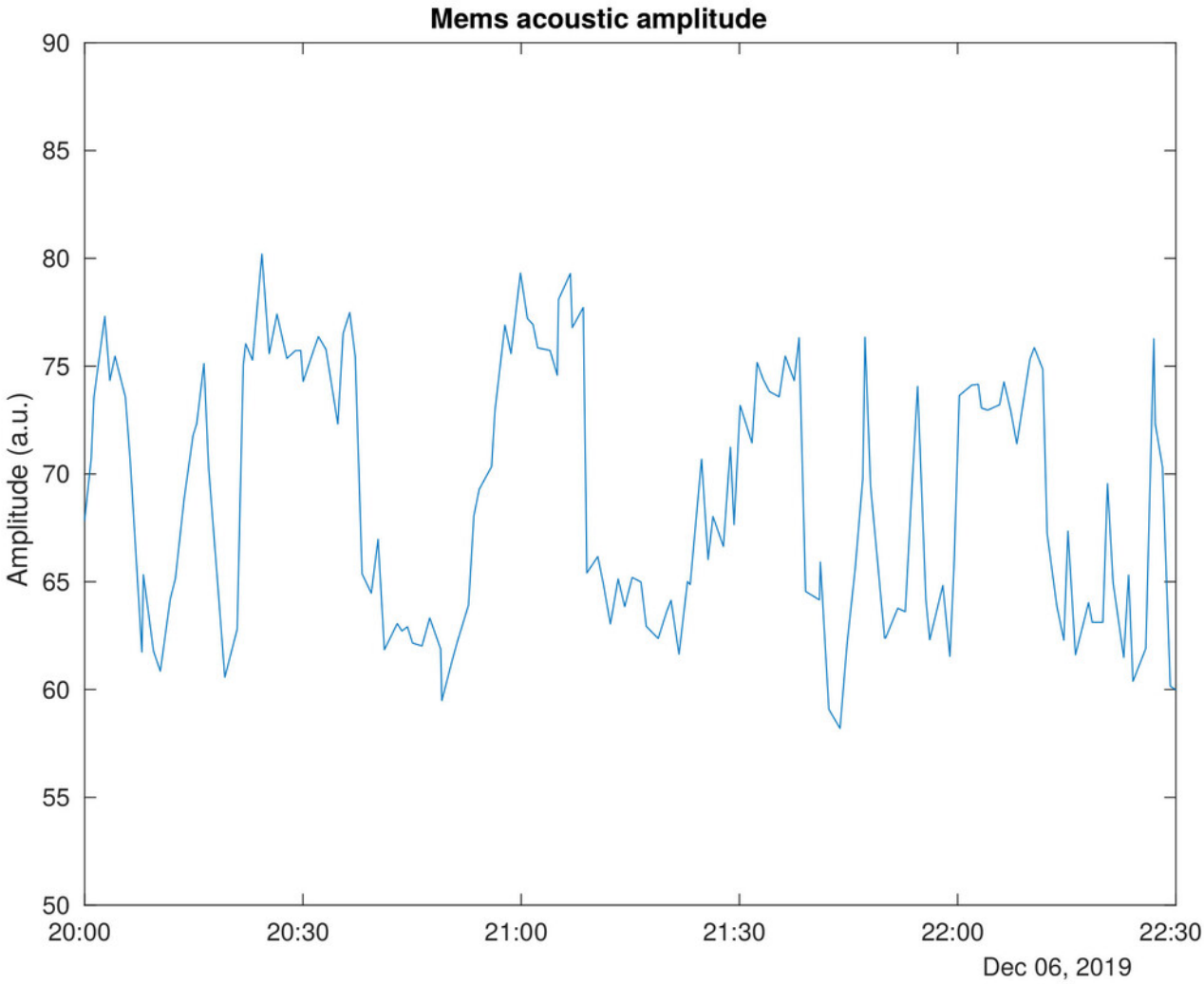

598
599 Figure 9 : Acoustic signal amplitude, measured 20 m away from the Pisciarelli fumarole between

600 20:00 and 22:30 (UTC) on 6 December 2019.